Journal of *Marine Science and Engineering*

MDPI

Article

A Data-Driven Method for Ship Route Planning Under Dynamic Environments

Zhaofeng Song [1,2,3], Jinfen Zhang [1,2], Chengpeng Wan [1,2] and C. Guedes Soares [3,*]

[1] State Key Laboratory of Maritime Technology and Safety, Wuhan University of Technology, Wuhan 430063, China; zhaofeng.song@tecnico.ulisboa.pt (Z.S.); jinfen.zhang@whut.edu.cn (J.Z.); cpwan@whut.edu.cn (C.W.)
[2] Intelligent Transportation System Research Center, Wuhan University of Technology, Wuhan 430063, China
[3] Centre for Marine Technology and Ocean Engineering (CENTEC), Instituto Superior Técnico, Universidade de Lisboa, 1049-001 Lisbon, Portugal
* Correspondence: c.guedes.soares@centec.tecnico.ulisboa.pt

Abstract

The paper proposes an improved A* Algorithm based on historical AIS data for the multi-objective optimisation of ship weather routes, explicitly focusing on optimising voyage distance, economic costs, and emission costs within Sulphur Emission Control Areas. The method utilises trajectory interpolation, Ordering Points to Identify the Clustering Structure, and the Douglas–Peucker algorithm to preprocess AIS data, thereby enhancing the flexibility and accuracy of multi-objective path planning. The method incorporates different cost weights and the time dimension to optimise different routes dynamically. The technique also optimises the route in real time by treating ship power as a decision variable, adjusting the power according to different task requirements. The proposed method is compared with other commonly used path planning algorithms within a specific maritime area. The results show that it offers better adaptability in terms of multi-objective costs and timeliness.

Keywords: weather routing; trajectory clustering; Douglas-Peucker algorithm; emission control area; multi-objective optimisation

check for updates

Academic Editors: Md Jahir Rizvi and Xinqiang Chen

Received: 3 August 2025
Revised: 20 September 2025
Accepted: 22 September 2025
Published: 3 October 2025

Citation: Song, Z.; Zhang, J.; Wan, C.; Guedes Soares, C. A Data-Driven Method for Ship Route Planning Under Dynamic Environments. *J. Mar. Sci. Eng.* **2025**, *13*, 1901. https://doi.org/10.3390/jmse13101901

Copyright: © 2025 by the authors. Licensee MDPI, Basel, Switzerland. This article is an open access article distributed under the terms and conditions of the Creative Commons Attribution (CC BY) license (https://creativecommons.org/licenses/by/4.0/).

1. Introduction

Maritime transportation serves as a vital component in facilitating worldwide commerce and fostering economic growth across nations, with an estimated 90% of global trade is transported by shipping [1]. Shipping is vital to human development and survival [2]. During voyages, ships emit large amounts of pollutants, such as PM2.5, CO_2, and SOx, further exacerbating environmental degradation [3]. Gas carrier operations account for a significant share of global transport emissions and are growing rapidly. To address this issue, the International Maritime Organisation (IMO) has defined numerous Sulphur Emission Control Areas (SECAs) in various regions [4] under the IMO 2020 regulations, imposing strict limitations on sulphur emissions within these designated areas [5]. Statistical analysis reveals that post-2020, maritime fuel sulphur concentrations demonstrate significant geographic variation: 0.10% in SECAs versus 0.50% in other maritime zones, reflecting IMO's tiered regulatory approach [6,7].

With its ability to provide real-time and historically accurate information, the use of AIS data can better plan maritime routes and enhance the understanding and optimisation of historical data, particularly in response to changing factors such as weather, traffic, and

risks. Accurate identification of high-density heading points [8] can quickly reflect course adjustments and provide critical data support for dynamic route optimisation.

1.1. Multi-Objective Path Planning

Energy conservation and emission reduction are becoming increasingly important in global transportation. In order to meet the above requirements, shipping companies usually use more expensive low-sulphur fuel [9,10]. However, high fuel costs place a considerable economic burden on shipping companies [11]. By optimising the vessel's weather routing [12], it is possible to reduce both economic and emission costs during the voyage effectively [13]. Some studies focus on accurately predicting meteorological information. These efforts are further integrated with heuristic methods and apply genetic algorithms for weather routing optimisation [14–16]. The improved Artificial Potential Field (APF) algorithm has also been widely used in multi-objective ship path planning. Reference [17] proposed an enhanced version called MTAPF, which divides the optimal local path into multiple sub-paths to avoid falling into local optima.

1.2. Path Planning Based on AIS Data

Against the accelerated development of electronic navigation and smart shipping [17,18], the Automatic Identification System (AIS) has been fully utilised in ocean ships. AIS is an automatic tracking system that identifies and locates vessels by exchanging data with nearby ships and AIS base stations. With the rapid development and convenience of AIS technology, maritime transportation can support remote vessel monitoring, intelligent scheduling, and autonomous navigation [19], thus improving the safety and efficiency of vessel operations [20]. Motivated by the above, this study analyses and mines large amounts of historical data, extracting patterns and features. Processing historical trajectory data quickly generates optimal paths and navigation strategies while adapting and optimising the route based on real-time data and situational planning [21].

Due to the complexity and variability of the marine environment, AIS devices may be unable to send or receive complete data when affected by signal interference or device malfunctions. Additionally, there may be specific errors in the location, speed, and heading parameters. In heavy-traffic waters, ships with AIS devices send exceptionally large amounts of data periodically [22–25]. To simplify, repair, and classify the massive AIS data, trajectory interpolation is employed to handle missing data, with repair accuracy exceeding 90% [26]. The Douglas–Peucker (DP) trajectory compression algorithm and its improved methods [21] have also been widely used. DP considers the shape of the ship's trajectory during compression, significantly reducing the compression time characteristics while preserving the original trajectory.

Another challenge in trajectory repair is removing noise points generated by signal communication issues when acquiring AIS data. The commonly used method for noise point removal is clustering-based approaches. Clustering algorithms mainly include K-means clustering [25], hierarchical clustering [23], and density-based clustering [26]. The DBSCAN algorithm has advantages such as not requiring predefined cluster numbers, the ability to discover clusters of arbitrary shapes and strong robustness. So, it has been widely applied to deal with AIS trajectory data.

1.3. Path Planning Considering Weather Conditions

The spatiotemporal variation in meteorological conditions is a key factor in route planning. Weather routing is a method of dynamically adjusting the speed or route based on meteorological conditions. Depending on the mission requirements, the ultimate goals of weather-based flight planning vary [27,28]. Building upon traditional heuristic and classical path planning algorithms such as LPA*, D*, and D-lite* [29–31].

In recent years, increasing attention has been paid to weather routing research that incorporates dynamic environmental factors. Wind [32], ocean currents [33], and waves [34] are key dynamic environmental factors increasingly focused on weather routing. The above factors will affect the various costs of ship navigation. A variety of techniques [35], including towing tank tests, CFD simulations, and semi-empirical methods, are commonly employed in ship model performance evaluations [36]. The integration of high-resolution meteorological information plays a key role in refining weather-based route planning. This type of environmental data also supports optimisation strategies such as heuristic and genetic algorithms [37], contributing to more reliable and efficient voyage predictions.

However, existing algorithms make only partial or no use of Automatic Identification System (AIS) navigation data to assist route planning, and they are unable to integrate historical AIS data with spatiotemporal meteorological information to support multi-objective route planning within Special Emission Control Areas (SECAs) [38]. Therefore, this study proposes an A* Algorithm based on historical AIS data in a dynamic marine Environment (A*-BAE). This multi-objective route planning algorithm better fits real AIS data and is designed for complex, dynamic marine environments and SECAs. The method leverages the relationship between speed and engine power to reduce algorithm runtime and rapidly generate the optimal route. The rest of this paper is organised as follows: Section 2 defines the problem; Section 3 introduces the AIS data and environmental source; Section 4 presents the main steps method; Section 5 discusses the results, simulations with different planning algorithms. Section 6 presents the conclusions and future research.

2. Problem Statement

Several challenges must be addressed before optimising ship routes under dynamic maritime conditions. First, extracting high-frequency heading points and detecting anomalies from AIS data ensures timely and precise support for route planning. Second, it is expected to autonomously develop cost-effective and environmentally friendly routes under complex maritime conditions to satisfy varying operational requirements. Third, this multi-objective path optimisation method can dynamically adjust engine power and optimise arrival time.

2.1. Trajectory Point Recognition Based on AIS Data

AIS data can better align with traditional empirical routes, providing real-time and historical data, and enhancing the understanding and optimisation of empirical routes. In practical applications, AIS data can offer dynamic support under complex conditions, especially in response to changing weather, traffic, and risk factors.

Using high-density heading points in AIS data can quickly identify the ship's adjusted direction and provide critical data support for dynamic route optimisation. Additionally, after removing anomalous data, AIS data can more accurately reflect ship's actual navigation path, making the planned route more aligned with real-world conditions [39]. Therefore, effectively integrating AIS data with route planning to enhance flexibility and accuracy has become increasingly important. Additionally, route planning and maritime analysis based on clustering and optimisation algorithms are becoming critical analysis.

2.2. Navigation Constraints Under Weather Routing

Under the IMO 2020 international regulations, ships must use fuel with a sulphur content not exceeding 0.5%. Moreover, cargo vessels increasingly focus on reducing emissions and managing fuel costs. To achieve significant reductions in SOx emissions, it is crucial to identify optimal routes and operational parameters. Freight vessels must be able

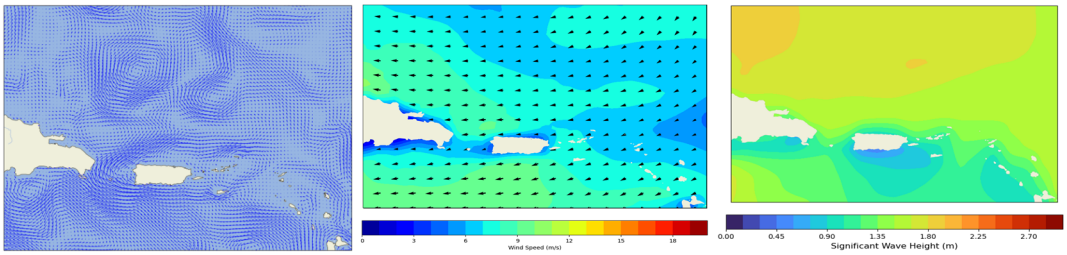
to generate routes that balance both cost and emission restrictions, ensuring efficient cost control while meeting emission reduction requirements.

2.3. Speed-Engine Power Under Multi-Object Navigation

Cargo ships often sail in windy areas and are greatly affected by currents, making their speed sensitive to environmental factors. While over 90% of open-sea navigation uses autopilot to maintain course, engine power is manually controlled and not adjusted in real time. In practice, changing marine conditions can cause fuel use and actual routes to deviate from initial plans. Therefore, optimising engine power along with route planning is key to improving efficiency. This helps shipping companies achieve more practical, efficient, and low-emission operations, enhancing both performance and safety.

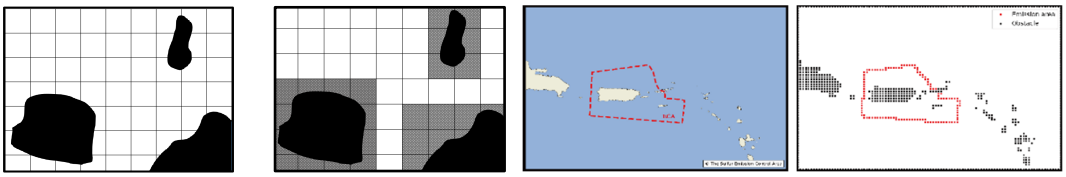
3. Data Source and Grid Map Construction

This study focuses on the same geographical area as our previous research, namely the United States Caribbean Sea, including the SECA. The shoreline data is obtained from Natural Earth, while meteorological inputs such as wind, waves, and currents are sourced from TideTech and ERA5. Both the map rasterization method and the meteorological data processing approach remain consistent with our previous study [40]. Figure 1 shows the processed meteorological data of different types. Figure 2 illustrates the raster map of the target area after processing. It should be specifically noted that, for the obstacle inflation rule, grid cells that are partially occupied also need to be marked as non-traversable areas.



(**a**) Current (**b**) Wind (**c**) Wave height

Figure 1. Meteorological data in [15–22 N, 70–60 W] [40] (Elsevier, 2025).



(**a**) Initialisation of the map. (**b**) Obstacle expansion. (**c**) Real environment map. (**d**) The grid map.

Figure 2. Grid map construction [40] (Elsevier, 2025).

The AIS data used in this study is from the National Oceanic and Atmospheric Administration (NOAA) Coastal Management Office (https://www.ngdc.noaa.gov/) accessed on 1 March 2025, which includes multi-dimensional ship data (real-time location, time, vessel type, speed, length, width, draft).

In the following case study, AIS data from [15–22 N, 70–60 W]. This area is a vital maritime route for traffic and trade between Central America and North and South America. The region's high transportation demand and emission restrictions provide reliable data support for the research presented in this paper. Figure 3 shows a visualisation of AIS trajectory points in the Caribbean region from 1 May 2022 to 1 June 2022.

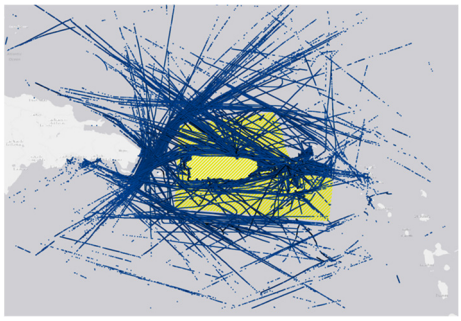


Figure 3. AIS trajectories from 1 May 2022 to 1 June 2022 in the Caribbean region.

4. Method

The flowchart of the multi-objective route optimisation method under sulphur emission restrictions is shown in Figure 4. This study aims to explore a more practical multi-objective route optimisation method based on AIS data, considering sulphur emission regulations, meteorological constraints, and the speed–power relationship. The method integrates and classifies ship data within the studied waters using AIS data and the OPTICS algorithm. The average core density calculation method is used to identify anomalous trajectory points. The DP algorithm is applied to extract high-frequency waypoints between different nodes.

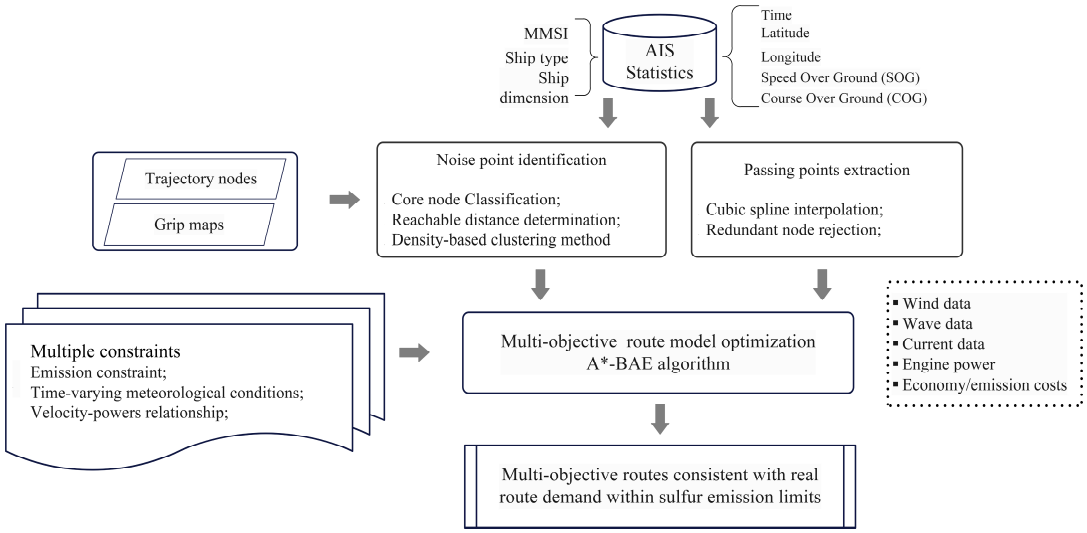


Figure 4. Flowchart of Multi-Objective Route Optimisation under Sulphur Emission Restrictions.

The improved A*-BAE algorithm determines the optimal distance, emission, and economic cost routes. Using the node vector relationship under dynamic weather conditions, the method balances the trade-off between ship speed and engine power to calculate the multi-objective cost function for different regions.

4.1. Data Processing Method

AIS data includes information such as ship position, course, speed, ship type, and more. This data can be used to monitor ship traffic, track ship positioning, and enhance safety management, ultimately improving maritime safety and efficiency. However, due to the complex marine environment and meteorological factors, AIS data may contain noise, missing values, and outliers. Therefore, effective data cleaning and repair are necessary before further analysis.

To address ship meteorological routing issues based on AIS data and environmental constraints, the following two aspects of AIS data need to be processed:

1. Recovery of Missing Data and Time Synchronisation: AIS data may deviate from the actual sensor measurements due to constant environmental changes. These deviations can result in variations in the AIS data broadcast frequency, leading to data loss and other issues. Additionally, AIS data from different sensors may not be synchronised in terms of time. Therefore, it is necessary to integrate inconsistent data formats from different AIS devices to provide unified data support for subsequent route planning. To repair the data, trajectory interpolation is used to restore missing AIS data.
2. Outlier Removal: Errors during data transmission from sensors can result in the generation of outliers or noise caused by factors such as equipment malfunctions, unexpected events, and other disturbances. Therefore, an algorithm is needed to establish relationships between data points and eliminate noisy points. The OPTICS algorithm can discover clustering structures based on the density relationships between data points and identify outliers by detecting anomalous points and improving data quality and reliability.

4.1.1. AIS Trajectory Processing Interpolation

AIS devices transmit data via VHF radio or satellite, but due to complex marine and weather conditions, the data often suffers from loss or distortion. Therefore, preprocessing is necessary. Linear interpolation is one of the most common methods for reconstructing AIS data. Since vessel trajectories are generally continuous and the dataset includes timestamps, positions, speed, and course, linear interpolation—being simple and efficient—can estimate missing values using just two known points. This makes it well-suited for initial AIS data processing.

Assume that the time series interval $[t_0, t_n]$ can be divided into $n + 1$ subintervals, with each waypoint corresponding to coordinates $[(x_0, x_1), (x_1, x_2), \ldots, (x_{n-1}, x_n)]$, and the corresponding function values are $[y_0, y_1, \ldots, y_n]$. Based on the dynamic AIS information at point (x_i, y_i), the vessel's estimated position at the interpolation point is then derived as follows.

$$\begin{cases} \mathrm{x}_i = x_1 + v_i \sin\theta_i (t_i - t_1) \\ \mathrm{y}_i = y_1 + v_i \cos\theta_i (t_i - t_1) \end{cases} \tag{1}$$

where v_1, θ_i and t_i represent the speed, sailing direction, and arriving time, respectively. Another predicted value for the ship position at the interpolation point obtained from the AIS dynamic information of point (x_j, y_j) is as follows.

$$\begin{cases} \mathrm{x}_j = x_2 + v_j \sin\theta_j (t_j - t_2) \\ \mathrm{y}_j = y_2 + v_j \cos\theta_j (t_j - t_2) \end{cases} \tag{2}$$

where v_j, θ_1 and t_j represent the speed, sailing direction, and arrival time at point (x_i, y_i), respectively. A weighted average is applied to the predicted values $(x_\mathrm{i}, y_\mathrm{i})$ and (x_j, y_j). The weights are assigned based on the relative time intervals between the interpolation point and the endpoints (x_i, y_i) and (x_j, y_j), with smaller time differences corresponding to higher weights.

The Gaussian coordinates of the interpolated point, obtained through weighted averaging, are given as follows

$$\begin{cases} \mathrm{x}_1 = Q_1 x_i + Q_1 x_j \\ \mathrm{y}_1 = Q_1 y_i + Q_1 y_j \end{cases} \tag{3}$$

where Q_1 and Q_2 denote the weights associated with endpoints (x_i, y_i) and (x_j, y_j), respectively. Ultimately, the AIS data values are reconstructed through interpolation. In this study, the linear interpolation method and steps were referenced from the research of [41].

4.1.2. OPTICS Clustering Algorithm

To guide route optimisation algorithms under dynamic weather conditions, vessel position information from AIS data is utilised to enhance the search process of an improved A* algorithm. According to the International Maritime Organisation, every ship is required to report AIS data every 2 to 12 s, depending on its speed. As a result, the volume of AIS data is enormous, especially in port areas. However, using all this data to inform the route optimisation algorithm is impractical. Only a subset of key nodes along the route can provide meaningful guidance to the algorithm. The OPTICS algorithm is applied to cluster vessel trajectories within port areas, addressing this challenge.

Specifically, the density-based OPTICS clustering algorithm is used to cluster ships. OPTICS does not specify the number of clusters generated, but instead orders the distances between different points during the classification process and iterates through updates. The distance for each point is composed of two values: core distance and reachability distance. The neighbourhood radius for the ship position dataset is denoted as ε, and Minpts refers to the minimum number of neighbouring ships required in each cluster. In this study, the ship point clustering method based on OPTICS, as proposed by [42], is referenced. The density of the ship $\rho(n)$ at node n can be represented as follows:

$$\rho(n) = |N\varepsilon(n)|, \tag{4}$$

The calculation methods for the reachability distance and core distance of the ship points are as follows:

$$Core_{\mathrm{d}}(n) = d(n, N_{\varepsilon}^{\min\ pts}), \tag{5}$$

$$Core_{\mathrm{d}}(n) = \begin{cases} \text{Undefined} & \rho(n) < \min\ pts \\ d(n, N_{\varepsilon}^{\min\ pts}) & \rho(n) \geq \min\ pts \end{cases}, \tag{6}$$

where $Core_{\mathrm{d}}(p)$ represents the core distance of point p, $N_{\varepsilon}^{\min\ pts}$ represents the minimum number of neighbouring ships per cluster, and nearest neighbours of node n. When assuming that node N is a core node, ensure that all $Core_{\mathrm{d}}(p) \leq \varepsilon$. The reachability distance is the shortest distance between a point outside a cluster and the nearest point within the neighbouring cluster. The calculation method is as follows:

$$Reach_{\mathrm{d}}(n, q) = \begin{cases} \text{Undefined} & \rho(n) < \min\ pts \\ \max(Core_d(n), d(n, q)) & \rho(n) \geq \min\ pts \end{cases}, \tag{7}$$

Figure 5 illustrates the core and reachability distance during the OPTICS iteration process. The red dashed line represents $Reach_{\mathrm{d}}(n, q)$ from the current node (the green grid in the figure), which refers to the furthest distance that the ship can travel from the current node to the target node cluster within a given time frame. The blue dashed line represents $Core_{\mathrm{d}}(n)$ between the ships within the cluster and other ships or obstacles.

Step 1: AIS data within the defined time window of the sulphur emission control area are extracted to construct ship trajectories, followed by initialisation of the neighbourhood radius ε and the minimum neighbour threshold (MinPts).

Step 2: When all points in the trajectory set **P** are processed, the algorithm terminates and outputs the trajectory points sequentially. Otherwise, an unprocessed core sampling point p is chosen and inserted into the result set **R**. The density-reachable points **N** of p

are then identified, and a new ordered set **Q** is created to incorporate these points for further processing.

Step 3: If **R** is non-empty, the smallest ship point is extracted from **Q**. When **Q** contains no elements, the neighbouring nodes are placed in **R**.

Step 3.1: Determine whether the nearest neighbour is a core point. If not, insert it into the result set **R** and proceed to Step 3.

Step 3.2: Determine if elements of **N** are included in **R**. If the newly calculated density-reachable point $Reach_{\mathrm{d}}(n,q)$ is smaller than the original $Reach_{\mathrm{d}}(n,q)$, update the $Reach_{\mathrm{d}}(n,q)$ value of that point and perform the same operation for the remaining points in **R**.

Step 3.3: If **R** lacks density-reachable points, add the point and repeat Step 3.

Step 4: Repeat steps 2–3 until all trajectory points and their corresponding $Reach_{\mathrm{d}}(n,q)$ values are obtained.

Step 5: Determine whether to cluster ships based on the size of ε, marking points with values greater than the threshold ε as outliers. The OPTICS process flow used in this study is shown in Figure 6.

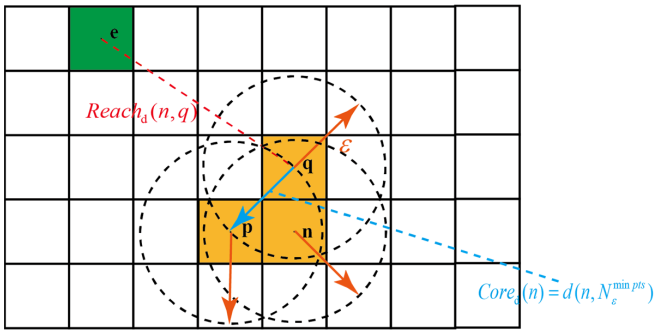


Figure 5. Schematic of the core and reachability distance during the OPTICS iteration process.

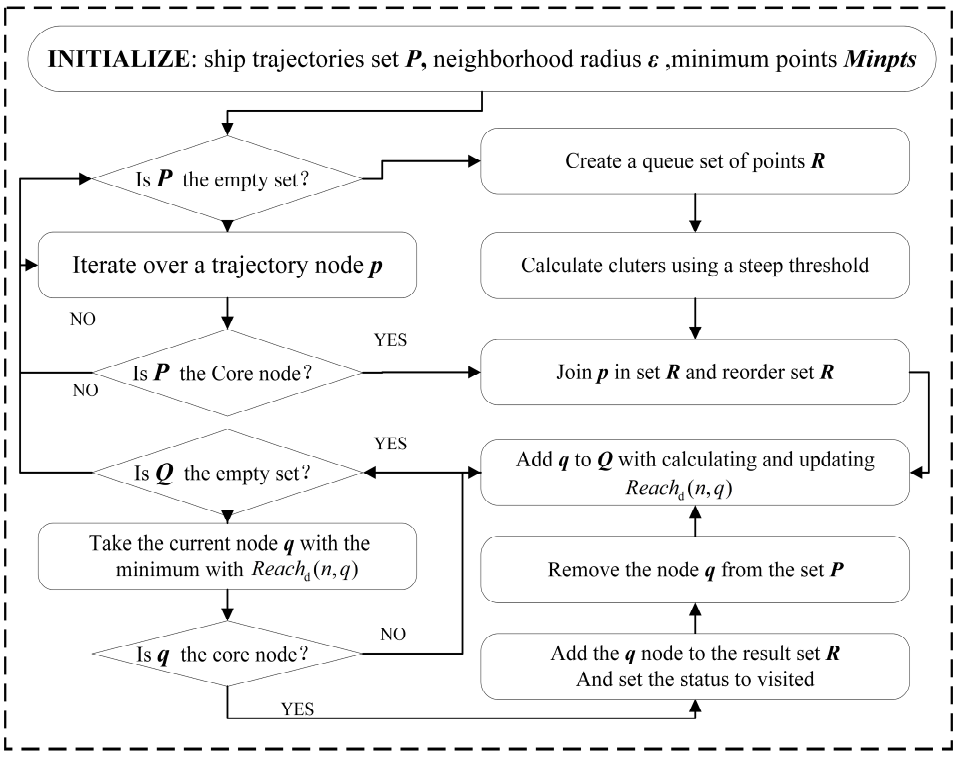


Figure 6. The OPTICS process flow.

It is important to note that to achieve a more accurate classification of high-density and low-density areas, the minimum is set to 3. Since the subsequent path search algorithm uses a heuristic approach, with the maximum distance between adjacent points in the algorithm being 1.414 basic units, then $\varepsilon = 1.414$. And we use the midpoint of the route nodes as the clustering centre. When initialising the core nodes in the OPTICS algorithm, the centre positions of the grid are designated as the initial core nodes for the subsequent iterative process. During the iteration, the OPTICS clustering procedure produces a structure in which nodes p, n, and q are grouped together to form a cluster, highlighted in yellow in the Figure 7. In contrast, node e is identified as an isolated outlier, visualised in blue, since its distance from the nearest cluster exceeds the predefined threshold ε. Within the context of this study, such isolated points are classified as noise, as they do not exhibit sufficient density connectivity with other nodes. This classification has direct implications for the subsequent path-planning algorithm. To enhance navigation safety and efficiency, the algorithm explicitly seeks to avoid trajectories that pass through or near these noise points, thereby reducing the risk of selecting anomalous or unreliable regions as part of the planned path.

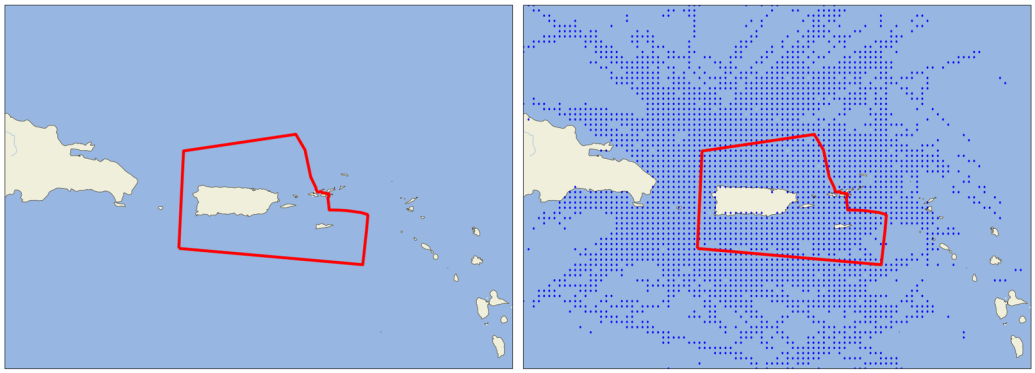


Figure 7. Initial case map and after clustering map (The red zone denotes the SECA).

4.2. Extract Turning Points

The DP algorithm was proposed by [43]. The DP algorithm recursively divides line data and uses a threshold to control compression quality. It is fast and accurate, making it widely used for simplifying movement trajectories and identifying turning points by detecting significant direction changes.

The main idea is to extract a set of key feature points, denoted as $N_s = \{N_1, N_2, N_3, \cdots, N_{m-2}, N_{m-1}, N_m\}$, from the original trajectory set, such that NS, under a certain threshold ε, closely resembles the original set.

The procedure of DP algorithm is shown in Figure 8. The red line segments represent d_{max} and the blue line segments represent ε.

Step 1: Represent the pre-processed trajectory point set as $N_t = \{N_1, N_2, \cdots, N_m\}$. The key feature point set is represented by N_s and initialised as an empty set.

Step 2: Traverse all trajectory points (including the starting and ending points). Assuming the line between the starting and ending points is the baseline, calculate the distance of all points to the baseline. Keep track of the maximum distance d_{max} and the corresponding node N_i. If the corresponding d_{max} of a point is greater than the threshold ϵ, then assign that point to the key point set N_s.

Step 3: At the segmentation point N_i, the trajectory is split and divided into two subsets N_{i1} and N_{i2}, where $N_{i1} = \{N_1, N_2, \cdots, N_i\}$ and $N_{i2} = \{N_{i+1}, N_{i+2}, \cdots, N_s\}$. If $d_{max} \geq \varepsilon$, then store it in the set N_s. In subsets N_{i1} and N_{i2}, further split at turning points to find the turning point corresponding to d_{max}.

Step 4: Repeat this process until the maximum distance d_{max} of all segmentation points is less than ε. The resulting set N_s is then the key set of turning points.

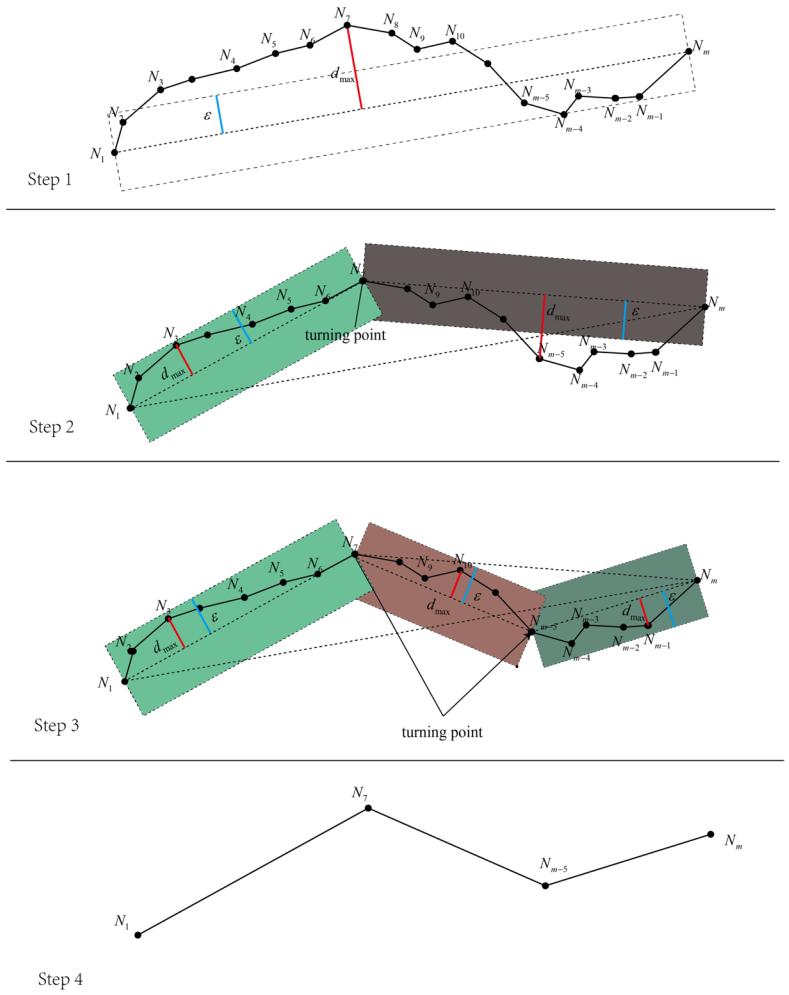


Figure 8. Schematic Diagram of DP Algorithm.

4.3. Multi-Objective Route Optimisation Method

4.3.1. Comparison of Multiple Algorithms

This study aims to utilise real-time and historical AIS vessel trajectory information to enhance safety and efficiency under varying spatiotemporal weather conditions, reduce emissions, and optimise operational costs by providing critical data support for dynamic route adjustments and decision-making. Traditional heuristic algorithms cannot meet such requirements, so an improved A*-BAE algorithm is used as a replacement for existing methods.

The traditional A* [44] algorithm optimises routes solely based on distance cost, whereas the A*-BAE algorithm incorporates environmental factors such as wind, waves, and currents between nodes. The method for integrating dynamic environmental information between nodes is described in [40]. Additionally, as shown in Figure 9, the traditional A* algorithm searches only in the eight surrounding directions, whereas A*-BAE can search preset non-adjacent turning points and generate the optimal path in terms of distance, emissions, and economics based on known weather conditions.

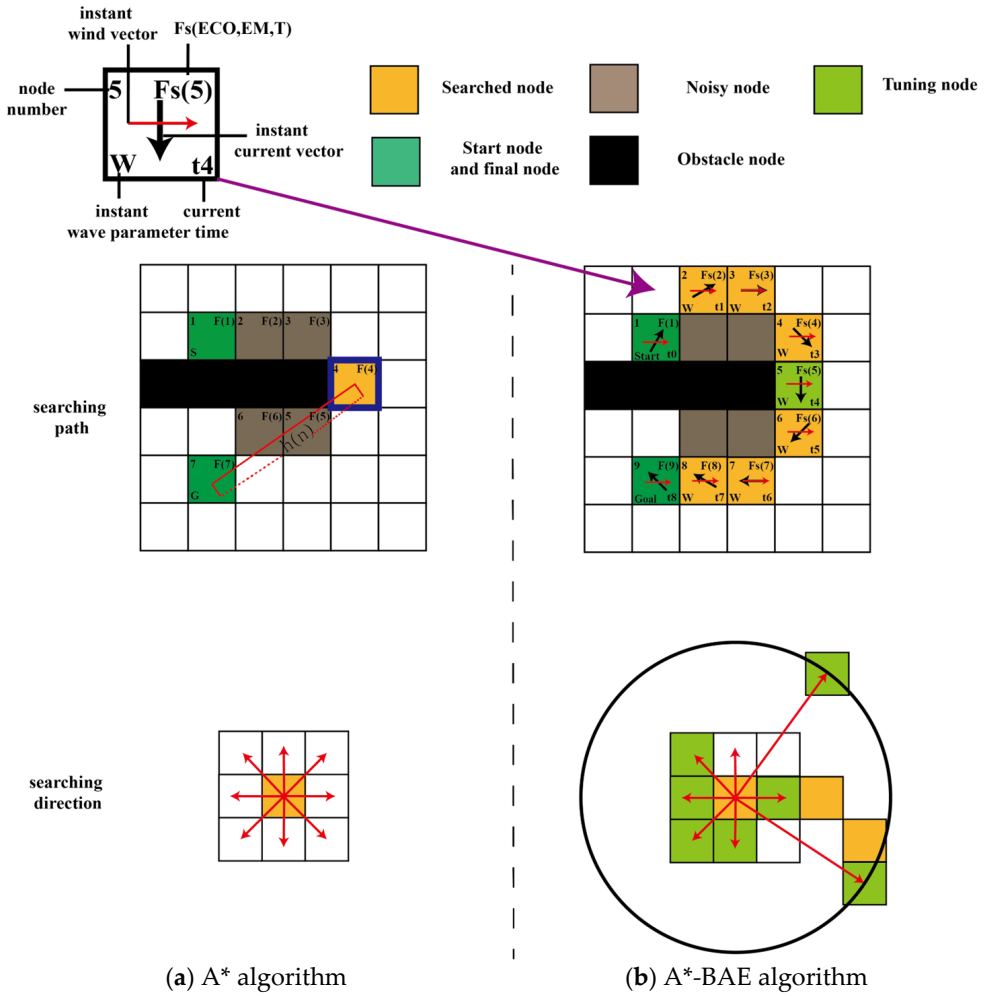


Figure 9. The search process of the A* and A*-BAE algorithms.

From Figure 9, it can be observed that this method can adapt well to the changing weather conditions. In A*-BAE, the vector relationships between nodes take into account dynamic meteorological conditions, as referenced in our previous research. The connection between the current node and neighbouring nodes follows the results of [40] to ensure the minimisation of the multi-objective costs.

In A*-BAE, the function $F^*(n)$ is introduced, where includes environmental factors and replacing the $F(n)$ of A* algorithm. $h'(n)$ is calculated using the following formula:

$$h'(n) = \omega_1 L_h + \omega_2 ECO_h + \omega_3 EM_h, \tag{8}$$

where the weights of the three costs are denoted by ω_1, ω_2 and ω_3, and $\omega_1 + \omega_2 + \omega_3 = 1$. These weights can be adjusted according to specific practical needs. L_h, ECO_h, and EM_h represent the estimated cost values from the current node to the destination. When calculating $g'(n)$ and $h'(n)$, it is necessary to normalise the different costs between the nodes. To ensure that the results fall within the range of [0, 1] with respect to the weight of each cost, the normalisation steps are as follows:

$$X = \frac{X - X_{\min}}{X_{\max} - X_{\min}}, \tag{9}$$

In this equation, X denotes the cost at n, while X_{min} and X_{max} represent the minimum and maximum costs at n. The updated method for calculating $g'(n)$, which takes meteorological conditions into account, is as follows:

$$g'(n) = g'(n_{par}) + \omega_1 L_g + \omega_2 ECO_g + \omega_3 EM_g, \quad (10)$$

In the formula, L_g, ECO_g, and EM_g represent the costs associated with travelling from the start to the current node.

4.3.2. Node Vector Transformation

To estimate economic and emission costs within ECAs, it is necessary to consider time and weather vectors across grid cells. These time-dependent costs are derived from vessel speed relative to both location and current. The vector-based calculation of ground-relative speed at different times and positions directly affects cost factors in route optimisation. The vessel's instantaneous speed at S_n is given by:

$$\vec{V}_{S_n t_{ng}} = \vec{V}_{S_n t_{nc}} + \vec{V}_{S_n t_n w} + \vec{V}_{S_n t_n r}, \quad (11)$$

where $\vec{V}_{S_n t_{ng}}$ represents the ship's speed over ground at time t_n. $\vec{V}_{S_n t_{nc}}$ and $\vec{V}_{S_n t_n w}$ represents the vector under current and wind, respectively. $\vec{V}_{S_n t_n r}$ represents the vessel's speed in calm water. Once the vessel's speed vector is defined, different costs can be dynamically analysed and optimised to achieve minimisation.

The connection methods between the current node and turning points in A*-BAE mainly include two types: 1. Adjacent node connection and 2. Non-adjacent turning point connection. For the adjacent node connection, the connection method refers to linking the centre of the current grid position to the centre of an adjacent grid position with a straight line segment and calculating various costs based on vector relationships. For non-adjacent turning point connections, the current node is treated as the starting point of A*-DCE [45], and multiple adjacent turning points are treated as the endpoint positions of A*-DCE, generating an optimal route with different cost objectives.

It is important to note that when generating sub-paths through A*-DCE, the weight factors must be consistent with those selected in the overall A*-BAE algorithm. The vector relationships between nodes in A*-BAE are illustrated in Figure 10, where the green nodes represent the set of nearest waypoints searched by the current passing point, and the yellow nodes are the critical points searched by the path planning algorithm.

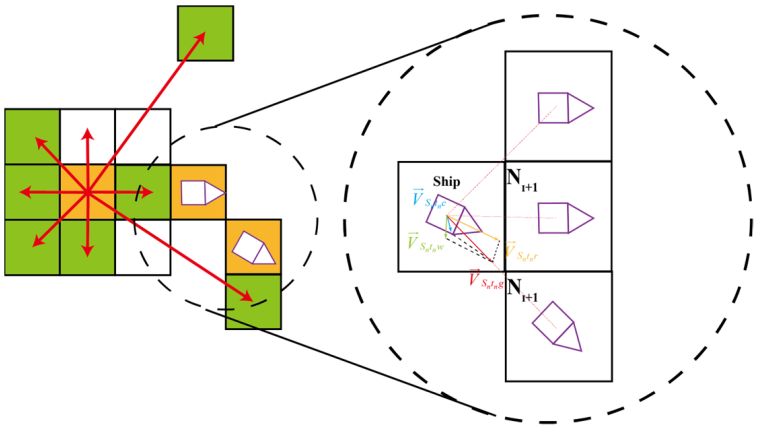


Figure 10. The vector relationship between waypoints.

4.3.3. Cost Functions

Defining different cost functions for a path to meet various task requirements under multiple constraints is important. Given the environmental and sulphur emission constraints. The cost function for distance L_{cost} is expressed as follows:

$$L_{cost} = \sum_{i=0}^{N} |N_i N_{i+1}|, \tag{12}$$

where represents the node i. The Haversine formula is applied to convert the Euclidean distance $|N_i N_{i+1}|$ into kilometres by using their longitude and latitude coordinates. The formula for this calculation is as follows:

$$\begin{aligned} |N_i N_{i+1}| = \quad & 3963.0 * arccos[(sin(LaN_i) * sin(LaN_{i+1})) \\ & + cos(LaN_i) * cos(LaN_{i+1}) * cos(LoN_{i+1} - LoN_i)] \end{aligned}, \tag{13}$$

where LoN_i and LaN_i denote the longitude and latitude of N_i, respectively. The economic cost is calculated as follows: (1) partitioning the vessel's maximum speed to support route optimisation under varying constraints; (2) deriving engine power based on vessel speed and resistance under environmental conditions; and (3) computing node-to-node costs by accounting for fuel type variations across regions. The detailed process is as follows:

Step 1: Speed zone classification. Following the approach of [40], the operational area is divided into three speed zones—low, medium, and high—according to the vessel's distance from surrounding obstacles. The corresponding classification results are illustrated in Figure 11.

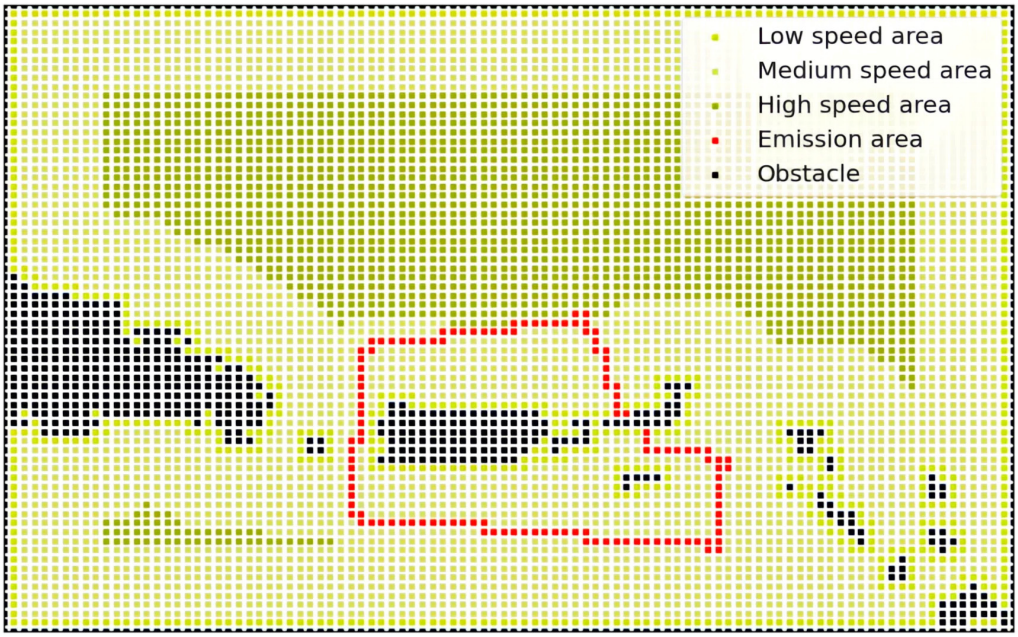


Figure 11. The regional velocity fields in the Caribbean [40] (Elsevier, 2025).

Step 2: Establishing the speed–power relationship. Engine output is influenced by the vessel's ground speed and dynamic environmental factors. Engine power P_b is computed based on vessel speed and average resistance F_r over time. The speed–power relation per unit time is expressed as follows:

$$P_b(U_{wind}, U_{current}, U_{wave}, V) = \frac{F_r(U_{wind}, U_{current}, U_{wave}, V) \cdot V}{\eta_p}, \eta_p = \eta_h \cdot \eta_o \cdot \eta_s \cdot \eta_r \tag{14}$$

where η_p, η_h, η_o, η_r, η_s represent the ship's propulsive efficiency, hull efficiency, open water efficiency, relative rotational efficiency and shaft efficiency, respectively. The ship's total resistance F_r in a dynamic environment can be approximated using the equation below:

$$F_r(U_{wind}, U_{current}, U_{wave}, V) = F_s + F_{wave} + F_{current} + F_{wind} \tag{15}$$

The variables F_s, F_w and F_c represent the basic resistance, the additional resistance or force caused by wind, and the added resistance due to currents, respectively. F_s can be computed as follows:

$$F_s = \frac{1}{2} C_0 \rho V^2 A_s \tag{16}$$

The parameters C_0, V, ρ, and A_s, correspond to the basic drag coefficient, fluid density, ship speed in calm water, and submerged area, respectively. The value of F_w can be computed using the following equation:

$$F_{wind} = \sqrt{F_{wx}^2 + F_{wy}^2} \tag{17}$$

$$F_{wx} = \frac{1}{2} A_h \rho_a C_w (V_{wrx}^2) \alpha_{wr} \tag{18}$$

$$F_{wx} = \frac{1}{2} A_h \rho_a C_w (V_{wrx}^2) \alpha_{wr} \tag{19}$$

where A_h, A_v, ρ_a, C_w, V_{wrx}, and V_{wry} represent the ship's sectional area, the reference area for wind drag, air density, the wind resistance coefficient along with the wind's horizontal and vertical velocity components, respectively. $\alpha_{wr} = \arctan\left(\frac{V_{wry}}{V_{wrx}}\right) - \varphi$, where φ represents the ship's heading angle at the node. $F_{current}$ denotes the resultant force exerted on the ship by the current at the node, which is calculated as follows:

$$F_{current} = \sqrt{F_{cx}^2 + F_{cy}^2} \tag{20}$$

$$F_{cx} = \frac{1}{2} \rho_c (V_{crx}^2) C_c A_h (\alpha_{cr}) \tag{21}$$

$$F_{cy} = \frac{1}{2} \rho_c (V_{cwy}^2) C_c A_v (\alpha_{cr}) \tag{22}$$

Parameters ρ_c, C_c, V_{crx}, V_{cry} represent water density, current resistance coefficient, and horizontal and vertical current velocities. Hull vertical forces arise from wind waves, seismic activity, and tides; this study focuses on resistance from regular waves. The disturbance force model is based on ship experiments and Daidola's empirical formula [34,46].

$$F_{cy} = \frac{1}{2} \rho_c (V_{cwy}^2) C_c A_v (\alpha_{cr}) \tag{23}$$

where $S(\omega | H_s, T_p)$ represents the wave spectrum at the node. Similarly, the economic cost $ECO_{\cos t}$ can be determined as follows:

$$ECO_{\cos t} = \sum_i^m \frac{L_i}{V_i} SFOC_{ECA} Pb_i P_{ECA} + \sum_j^n \frac{L_j}{V_j} SFOC_{NECA} Pb_j P_{NECA} + E_{add} \tag{24}$$

where $SFOC_i$ and $SFOC_j$ represent the ship's Specific Fuel Oil Consumption in different areas, respectively. P_i and P_j refer to the corresponding fuel price. E_{add} represents additional voyage costs, including maintenance, crew salaries, port fees, life-cycle costs, and administrative expenses. Since the variation in fuel prices does not affect the result of route optimisation, the method for selecting [47] and regional fuel follows the reference.

The emission cost is Calculated as follows:

$$EM_{\cos t} = \sum_{i}^{n} \frac{L_i}{V_i} SFOC_{NECA} Pb_i EF_{ECA} + \sum_{j}^{m} \frac{L_j}{V_j} SFOC_{NECA} Pb_j EF_{NECA} \quad (25)$$

where EF_i and EF_j denote the sulphur content within ECA and non-ECA regions, respectively. Figure 11 indicates the regional velocity fields in the Caribbea area.

4.3.4. Matching Mechanism Between the Dynamic Environment and the Grids

To better integrate the spatiotemporal variations in marine conditions with historical AIS data, the A*-BAE algorithm proposed in this study introduces spatiotemporal variations in meteorological conditions to achieve more accurate multi-objective path planning. Figure 12 illustrates the matching mechanism of spatiotemporal variations in wind, waves, and currents introduced into the grid by the algorithm.

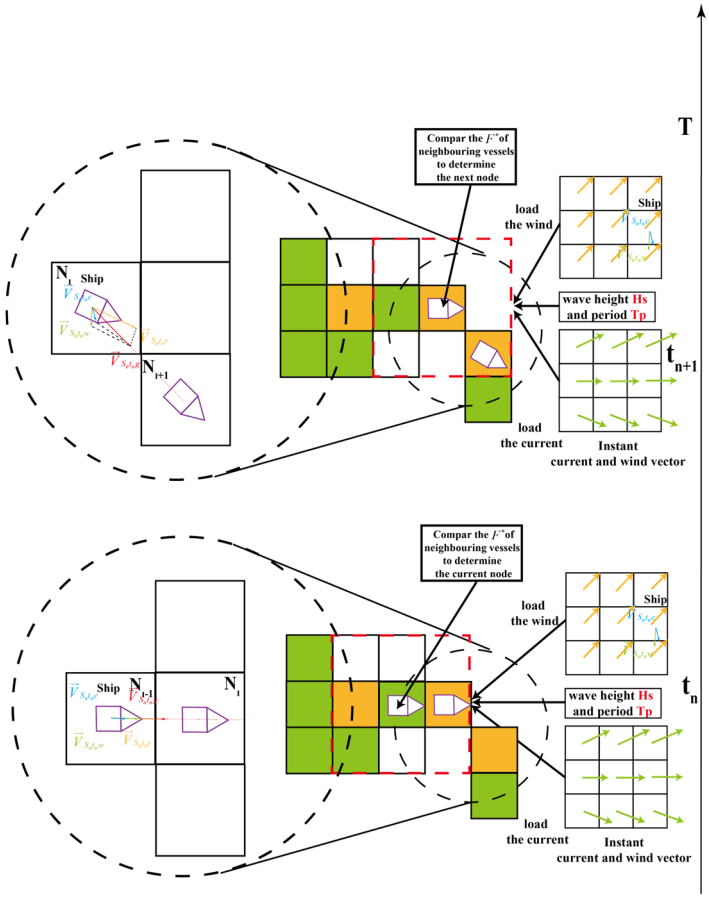


Figure 12. Spatiotemporal matching mechanism for wind, wave, and current.

The specific steps are as follows:

(1) The starting point is set as the current node, and the eight nearest waypoints to the current node are traversed, with the meteorological conditions at the current moment being imported for each node.

(2) Each of the eight nodes is sequentially set as the destination, with the current node as the starting point. The optimal path is planned using the A*-BAE algorithm, and the specific steps for planning the optimal path are as follows:

(2–1) Node-to-node cost calculation yields $F^*(S_n)$ and the optimal arrival times to adjacent nodes.

(2–2) Set the node with the lowest cost as the starting point for the next search and update the current node's start time. The costs for travelling from the current node to the next node are recorded. The optimal path and cost connecting this node are stored.

(2–3) The meteorological conditions are reloaded based on the updated time, and steps (2–1) and (2–2) are repeated. During the search, if any of the 8 neighbouring nodes have a lower cost than previously calculated, their path and cost are updated. This continues as updated nodes become new starting points. Cumulative costs are recorded, and the optimal path for each route is identified.

(3) Select the waypoint as the next node which is referred to as the minimum cost. Repeat step (2) until the destination set by the model becomes the current node. Once this happens, stop searching this node and record the optimal path and cost connecting it.

(4) Reload the meteorological conditions based on the updated time and repeat steps (1) to (3). During the search, if a neighbouring waypoint has a lower cumulative cost than before, its path and cost are updated. This process continues until the destination becomes the new starting point. The total costs are recorded, and the final path is taken as the optimal route.

5. Case Studies and Discussion

5.1. Optimisation of Route and Model Parameters

AIS data is selected from ship routes within the U.S. Caribbean region, covering the area over [15–22 N, 70–60 W]. The AIS data CSV file contains 1,610,385 rows and 17 columns. The columns of the dataset consist of the following attributes: 'MMSI', 'BaseDateTime', 'LAT', 'LON', 'SOG', 'COG', 'Heading', 'VesselName', 'IMO', 'CallSign', 'VesselType', 'Status', 'Length', 'Width', 'Draft', 'Cargo', and 'TransceiverClass'. The meteorological data follows the same time span as the sailing period. After preprocessing the meteorological data in Section 2.1, dynamic environmental data is refined to a 1 h interval with an accuracy of 0.1°. The type of fuel used in different regions affects the optimal route selection based on various expected costs [48]. However, this study primarily focuses on route planning methods, so the choice of fuel does not influence the effectiveness of the route planning approach. Shipping companies commonly comply with sulphur emission regulations by using fuels with varying sulphur contents in different zones [49]. Marine gas oil (MGO) containing 0.10% sulphur is employed within SECAs, whereas low-sulphur fuel oil (LSFO) with 0.50% sulphur is used outside ECAs. The vessel was selected owing to its wide operating range, prolonged service duration, and notable environmental relevance, aligning well with the research objectives. The ship's characteristics and parameters are listed in Table 1. Actual ship routes from AIS data are used to verify the algorithm's effectiveness, with the selected route including a ship that passes through SECAs. Specific parameters for this ship are provided in Table 2. All experiments were conducted on a system equipped with an Intel Core i7-11800H processor, an NVIDIA GeForce RTX 3060 Laptop GPU, and 16 GB of memory. The software environment was implemented using Python 3.8.

Table 1. IONIC ALTHEA characteristics.

MMSI	Vessel Name	IMO	Vessel Type
538007953	IONIC ALTHEA	IMO9728435	Crude Oil Tanker
Length	Width	Height	Draft
250	44	42.08	8.3
Tonnage	Engine power		
63,771	11,730		

Table 2. Main Characteristic Parameters.

Parameters	Value	Unit
η_p	0.85	
L	250	m
B	44	m
H	42.08	m
Design draught	10.98	m
A_s	11,000	m^2
A_v	1851.52	m^2
A_h	10,520	m^2
C_0	0.8	
ρ	1000	kg/m^3
ρ_a	1.225	kg/m^3
C_w	1.2	
C_c	0.9	
α_{wr}	0.9	
SFOC at 85%MCR	173	(g/kWh)
PMGO	547	$/ton
PLSFO	585	$/ton
EFI	1.81	g/kWh
EFJ	9.05	g/kWh

5.2. Multi-Objective Path Optimisation

Four different scenarios are set for comparative testing to evaluate the performance of the route optimisation method under predefined starting points, endpoints, and estimated time of arrival (ETA) constraints. The starting times for these scenarios are 00:00:00 on 1 May 2022, 00:00:00 on 6 May 2022, 00:00:00 on 9 May 2022, and 00:00:00 on 12 May 2022.

To examine the influence of different start and end points on the route planning results, the first two scenarios use the same start and end points as the selected real route, i.e., from 15.5° N, 68.9° W to 20.7° N, 64.3° W. The latter two scenarios use 20.7° N, 64.3° W to 15.5° N, 68.9° W as the start and end points. The meteorological data and real route data required for route optimisation are provided by the meteorological bureau and AIS data described in Section 3.

To validate and compare the performance of the proposed A*-BAE method, two widely studied route planning methods, A* and RTAA* [50], are also introduced. It should be noted that the real route data were obtained through data preprocessing (including outlier removal and resolution reduction), while the traditional A* and RTAA* algorithms use their own algorithmic logic to optimise the path with distance as the objective. The fundamental principle of these methods lies in generating a target path from a specified start node to a final node, along with obstacle constraints, and then solving three cost functions by incorporating meteorological data.

To ensure equitable evaluation, the cost model presented in Section 3 is applied uniformly to assess all three route planning approaches. Since meteorological forecasts provide multi-day predictions, the dependency on identical weather data for both actual and optimised routes does not compromise the validity of their comparative analysis. Additionally, since the VNSS system updates the forecast data every 24 h during the actual voyage, and the meteorological model can predict ocean conditions for the next 3–5 days (especially in international waters), it is reasonable to assume that differences in meteorological input optimisation will not impact the comparison results. Tables 3 and 4 show the different costs comparisons for various planned routes in different scenarios to observe the cost comparisons under different scenarios visually.

Table 3. Costs of different route optimisation methods at 05-03.

Number	Start Time	Method	Weight/[w1, w2, w3]	Distance Cost (km)	Economic Cost ($)	Emission Cost (Ton)
1	05-03	Actual path	/	857.25	21,930.74	354.11
2	05-03	A* path	/	826.40	18,829.47	292.49
3	05-03	RTAA* path	/	857.88	21,851.60	361.53
4	05-03	Smallest distance path	[0.97, 0.01, 0.02]	826.80	18,312.86	281.39
5	05-03	Greatest distance path	[0.00, 0.00, 1.00]	937.47	23,321.79	276.14
6	05-03	Most economic cost path	[0.61, 0.25, 0.14]	826.89	18,250.05	280.35
7	05-03	Highest economic cost path	[0.00, 0.00, 1.00]	937.47	23,321.79	276.14
8	05-03	Lowest emission path	[0.26, 0.00, 0.74]	880.07	20,318.98	270.30
9	05-03	Highest emission path	[0.00, 0.85, 0.15]	851.67	19,449.60	321.78

Table 4. Costs of different route optimisation methods at 05-06.

Number	Start Time	Method	Weight/[w1, w2, w3]	Distance Cost (km)	Economic Cost ($)	Emission Cost (Ton)
1	05-06	Actual path	/	857.25	23,164.59	372.40
2	05-06	A* path	/	826.40	17,562.23	252.31
3	05-06	RTAA* path	/	857.88	20,287.3	335.65
4	05-06	Smallest distance path	[0.97, 0.01, 0.02]	826.80	18,461.91	283.86
5	05-06	Greatest distance path	[0.00, 0.03, 0.97]	951.99	23,100.94	272.49
6	05-06	Most economic cost path	[0.61, 0.25, 0.14]	826.89	18,399.10	282.82
7	05-06	Highest economic cost path	[0.00, 0.00, 1.00]	951.92	23,258.56	276.04
8	05-06	Lowest emission path	[0.00, 0.03, 0.97]	951.99	23,100.94	272.49
9	05-06	Highest emission path	[0.13, 0.74, 0.13]	851.67	19,598.65	324.25

The simulation results for the four scenarios are shown in Figure 13. It indicates that the A-BAE algorithm can generate optimal paths while considering the ship's multi-objective factors, providing ship owners with multiple route alternatives. Additionally, A-BAE is capable of achieving the optimal costs. When considering distance cost, the path generated by the A*-BAE algorithm is almost identical to the one generated by the traditional A* algorithm, which only optimises the distance. This is because the weight generated in the algorithm's iterations is closer to the weight used in the traditional A* algorithm.

In terms of economic cost, the path generated by the A*-BAE algorithm considers regions where meteorological conditions have less impact, thereby reducing engine power and fuel consumption. The maximum reductions in economic cost for the optimal paths generated in the two scenarios are 16.8% and 20.6%, respectively, resulting in significant reductions in the ship owner's financial expenditure. For emission costs, the path generated by the A*-BAE algorithm can either pass through or avoid emission control areas (SECAs) to achieve optimal costs. The maximum reductions in emission costs for the optimal paths in the two scenarios are 23.7% and 26.8%, respectively.

In summary, by comparing the path generation capabilities of the algorithm across different scenarios and the candidate paths generated by A-BAE can meet the experimental requirements.

As shown in Tables 3 and 4, the shortest distance paths for the ship remained unchanged, but both economic and emission costs decreased. This is because changes in meteorological conditions affect engine power when the ship sails along a fixed route. The path generated by Algorithm A has a distance cost of 810.99 km In summary, the algorithm proposed in this study can effectively reduce other costs while ensuring a certain level of distance optimality.

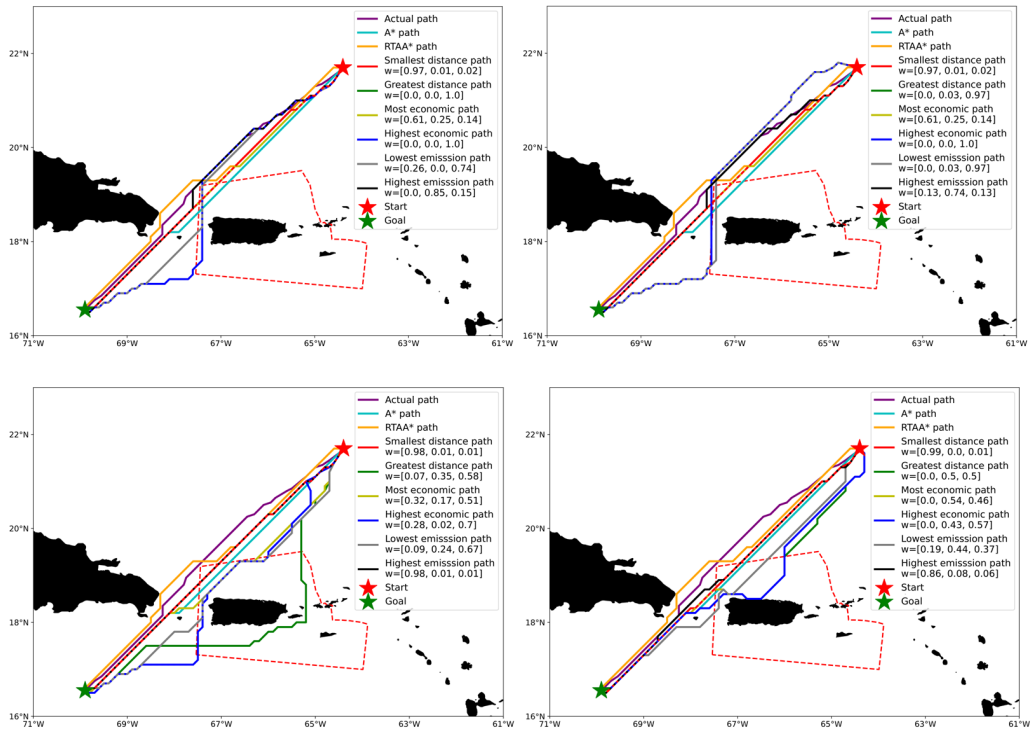
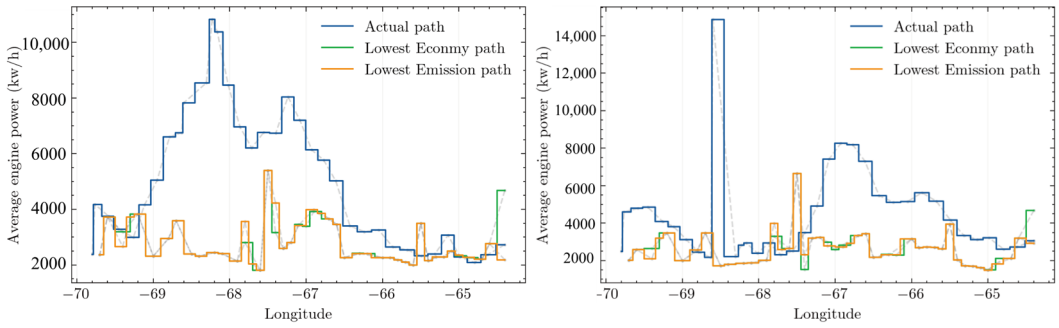


Figure 13. Visualisation results of routes with different starting times and locations.

When environmental conditions change over time, the ship will autonomously choose routes with less resistance, thus reducing multi-objective costs. If the ship follows the optimised path generated by the A* algorithm or the method proposed in this study, it may partially pass through SECAs compared to the empirical route. Although fuel consumption (SFOC) increases in SECAs, the overall performance improves due to the reduced total distance, better speed distribution, and lower power required to overcome resistance.

5.3. Real-Time Power Comparison Under the Optimal Path

To observe the effects of optimised paths on economics and emissions in more detail, Figure 14 presents a comparison of the actual path, the most economical path, and the path with the lowest emissions, with results for different departure times also compared. Although the trajectories of the optimised paths differ, the starting and ending longitudes, as well as the overall route, remain consistent. The horizontal axis represents the longitude travelled by the ship, while the vertical axis shows the ship's actual power, allowing for a visual representation of its adaptability in dynamic marine environments.



(**a**) 2022-05-03 00:00:00 (**b**) 2022-05-06 00:00:00

Figure 14. Real-time engine power of the optimal path for different cost objectives.

In Figure 14, each step length indicates how far the ship moves in longitude per hour. In the initial phase of the voyage, the actual paths under different departure times are nearly identical to the optimal economic and lowest-emission routes. Since the ship has not yet entered the SECA in the early stage of the voyage. Moreover, the proposed method incorporates meteorological effects into route planning, unlike the empirical path, enabling the ship to follow the path of least resistance.

During the middle stage of the voyage, the optimal economic and lowest-emission routes generally require less power than the actual route, as the ship slows near obstacles to avoid collisions (Section 2.3). The proposed method further reduces economic and emission costs by routing through the sulphur emission control area, shortening the voyage distance and lowering operational expenses.

In the final phase of the voyage, it is similar to the initial phase of the journey. By this time, the ship has exited the sulphur emission control area and is sailing at the pre-set speed. The primary distinction between the optimal paths for various objectives and the actual path is the consideration of meteorological conditions, resulting in minor variations in engine power.

5.4. Comparison of Trajectory Points Based on AIS Data

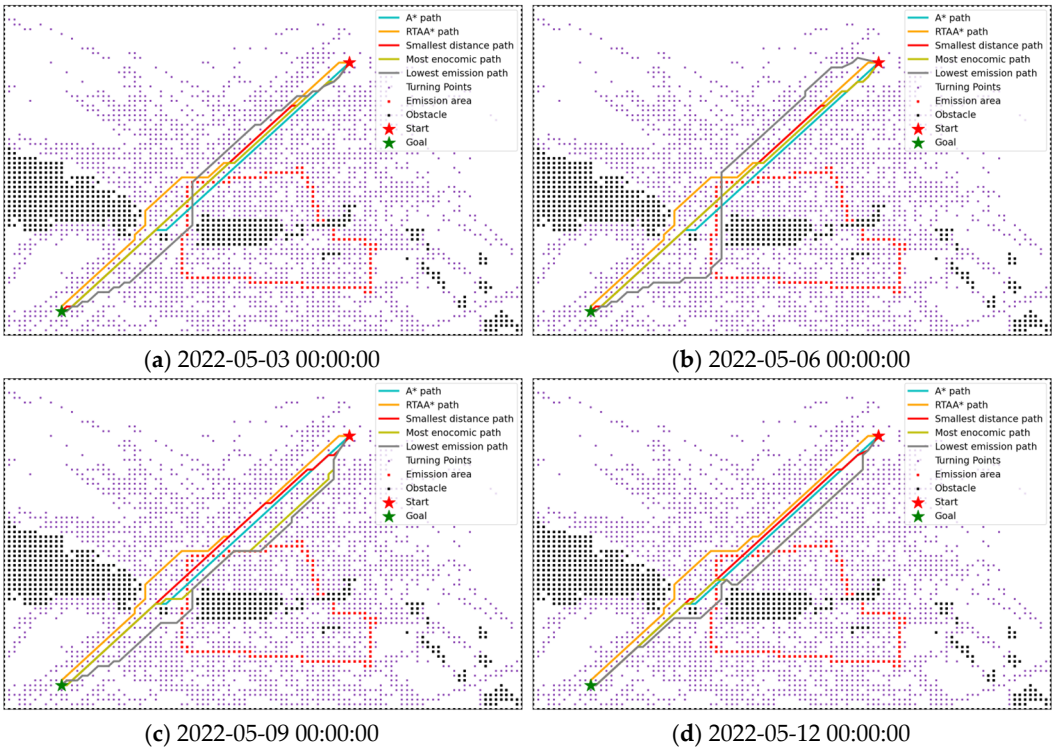
To verify the overlap between the proposed method and AIS data, four different optimal paths are designed for four departure times (05-03, 05-06, 05-09, 05-12). For each starting time, the A*-BAE method is used to generate the optimal distance path, optimal economic path, and optimal emission path for comparison. Traditional methods, including the heuristic A* algorithm and the learning-based RTAA* algorithm, were also used for comparison under different objectives. To demonstrate that the proposed algorithm can perform node search based on pre-processed AIS data, the globally optimal routes are present at the four aforementioned time instances after node refinement using DP algorithm, as shown in Figure 15. The alignment between heading directions and turning points across different algorithms is further analysed. For the four time periods, most of the trajectory points generated by the A*-BAE algorithm overlap with the turning points, whereas the traditional A* and learning-based RTAA* algorithms conduct their searches across the entire node space without leveraging such prior knowledge. This reflects that AIS data can serve as valuable prior information for the A*-BAE algorithm, providing directional guidance within the target region and significantly accelerating the global optimisation process.

To assess the overlap of each path with AIS data, the AIS data grid points for this scenario are first computed using three spline interpolations, OPTCS, and DP algorithms. Next, the number of nodes in each path are compared with the percentage of overlapping nodes from the AIS data points. The comparison of track points between the four different starting times is shown in Figure 16.

The number of nodes refers to the total number of searched nodes along the entire path. The number of repeated nodes represents how many of the traversed nodes coincide with the nodes refined by the DP algorithm. Although the A*-BAE conducts its search based on a filtered subset of nodes, we include all intermediate nodes between two adjacent refined points that pass through the original grid-based map to ensure a fair comparison of the overall path. The percentage occupied is defined as the number of overlapping nodes divided by the total number of nodes in the path.

By examining Figure 16, the multi-objective path generated by the A*-BAE method is comparable to the traditional A* search method in terms of node count for the distance metrics, while the path searched by RTAA* is slightly higher than the two methods mentioned above. This is because RTAA* performs real-time path search, continuously adjusting the

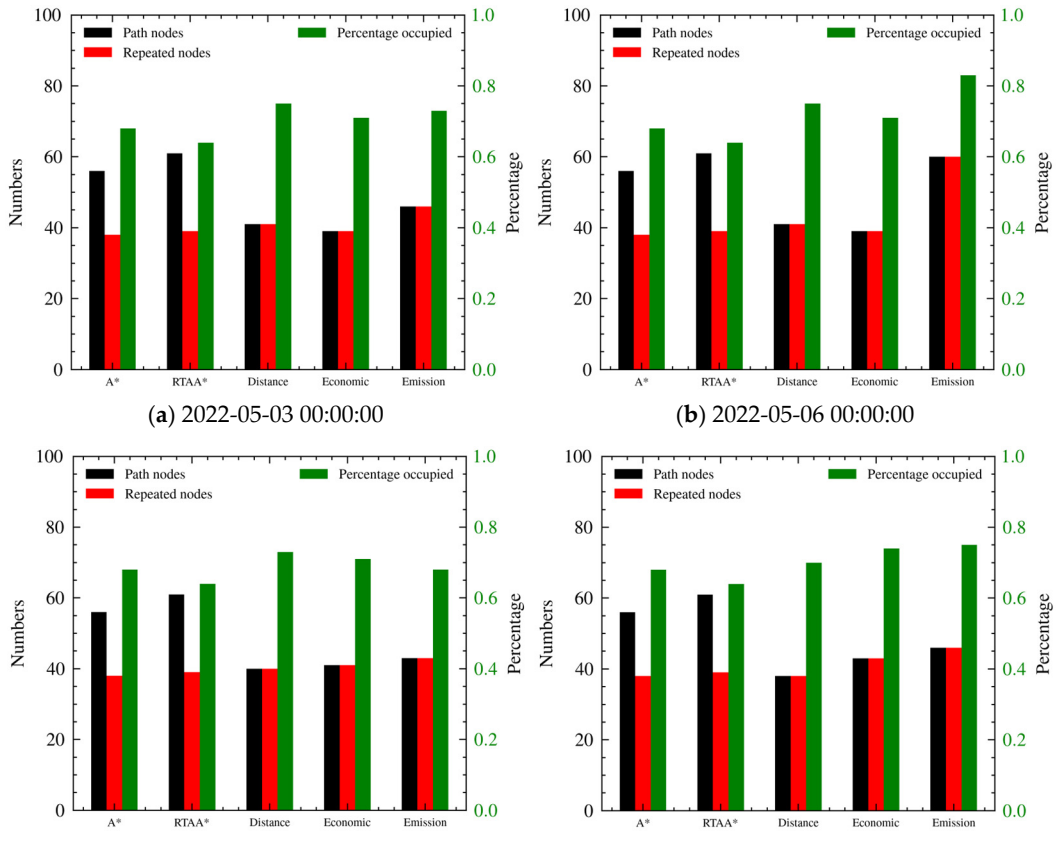
path during each search to ensure optimality in the distance metric (see 2022-05-06 00:00:00 in Figure 16).



(**a**) 2022-05-03 00:00:00 (**b**) 2022-05-06 00:00:00

(**c**) 2022-05-09 00:00:00 (**d**) 2022-05-12 00:00:00

Figure 15. Comparison of route optimisation results and turning points for different starting times.



(**a**) 2022-05-03 00:00:00 (**b**) 2022-05-06 00:00:00

(**c**) 2022-05-09 00:00:00 (**d**) 2022-05-12 00:00:00

Figure 16. Comparison of the waypoints of optimal paths from various algorithms.

However, compared to methods that find the optimal result with a single search, RTAA* performs slightly worse. Furthermore, the node count for the other two cost metrics in the A*-BAE method is also comparable to traditional methods. This indicates that while the method sacrifices a certain degree of computational efficiency and timeliness, it reduces the economic and emission costs of the optimal path. This demonstrates that the proposed method has a significant advantage in terms of runtime performance. In terms of the overlap with real routes, the search node count of A*-BAE is no more than 12.5% higher compared to the traditional A* method that considers spatiotemporal changing ocean conditions.

In addition, compared to traditional path planning algorithms, the DP algorithm preserves the original AIS trajectory shape features in the optimised path. This allows the algorithm to pass through a certain number of important waypoints at each node, ensuring that the AIS data points are not bypassed, regardless of the threshold, in order to achieve better optimisation results.

The paths planned by the method proposed in this study achieve over 96% overlap with the AIS data, as the method filters out anomalies during the grid division process and tends to select frequently occurring trajectory points during the optimisation process. This enhances the understanding and optimisation of the empirical routes. Moreover, the method can adapt to changing factors such as weather, flow, and risks. Based on the accurate identification of high-density waypoints, it can quickly reflect the ship's directional adjustments and provide key data support for dynamic route optimisation. It can also optimise objectives for both emissions and economics.

6. Conclusions

This study proposes a novel A*-BAE method to solve the multi-objective route optimisation problem by including historical ship trajectory data. It uses the average engine power over a unit time as the decision variable and plans routes that balance economic and environmental considerations based on AIS data. The advantage is that it navigates according to specified power and routes and optimises multiple objectives by referring to historical AIS routes, generating optimal paths under spatiotemporal changing ocean conditions.

By using meteorological and AIS data from different dates in the Caribbean Sea in 2022 as a reference, the adaptability of this method to spatiotemporal changes in ocean conditions and its alignment with historical data were validated. The A*-BAE method is compared with actual routes, A* algorithm, and RTAA method in terms of cost and waypoint coverage. The results show that the A*-BAE method achieved reductions of 20.6% and 26.8% in economic and emission costs, respectively.

In terms of overlap with real routes, the search node count of A*-BAE is no more than 12.5% higher compared to the traditional A* method, which considers spatiotemporal changes in ocean conditions. Moreover, this method can generate globally optimal routes with the lowest distance, economic, and emission costs, considering the ship's engine power over a specified time unit.

Author Contributions: Conceptualization, Z.S., J.Z. and C.G.S.; methodology, Z.S.; software, C.W.; validation, Z.S., J.Z. and C.G.S.; formal analysis, Z.S.; investigation, J.Z.; resources, C.W.; data curation, C.G.S.; writing—original draft preparation, Z.S.; writing—review and editing, Z.S.; visualization, J.Z.; supervision, C.W.; project administration, C.G.S.; funding acquisition, J.Z. All authors have read and agreed to the published version of the manuscript.

Funding: The research is financially supported by the National Key Technologies Research & Development Program (2023YFB4302303), Guangxi Natural Science Foundation (2025GXNSFHA069259), the Key Research and Development Program of Guangxi Zhuang Autonomous Region (Guike2023AA14003) and the Guangxi Science and Technology Program (AB23026132). It also contributes to the Strategic

Research Plan of the Centre for Marine Technology and Ocean Engineering (CENTEC), funded by the Portuguese Foundation for Science and Technology (Fundação para a Ciência e Tecnologia—FCT) under contract UIDB/UIDP/00134/2020.

Data Availability Statement: No new data were created or analyzed in this study.

Conflicts of Interest: The authors declare no conflict of interest.

References

1. Wu, Y.; Wang, T.; Liu, S. A Review of Path Planning Methods for Marine Autonomous Surface Vehicles. *J. Mar. Sci. Eng.* **2024**, *12*, 833. [CrossRef]
2. Park, M.-H.; Yeo, S.; Kim, J.-H.; Choi, J.-H.; Lee, W.-J. Comprehensive Review on Recent Progress in Renewable and Sustainable Energy Applications in Shipping Industry, and Suggestions for Future Developments. *Renew. Sustain. Energy Rev.* **2026**, *225*, 116152. [CrossRef]
3. Sun, Y.; Yang, L.; Zheng, J. Emission Control Areas: More or Fewer? *Transp. Res. D Transp. Environ.* **2020**, *84*, 102349. [CrossRef]
4. Tadros, M.; Ventura, M.; Guedes Soares, C. Review of the IMO Initiatives for Ship Energy Efficiency and Their Implications. *J. Mar. Sci. Appl.* **2023**, *22*, 662–680. [CrossRef]
5. Xia, J.; Wang, K.; Wang, S. Drone Scheduling to Monitor Vessels in Emission Control Areas. *Transp. Res. B Methodol.* **2019**, *119*, 174–196. [CrossRef]
6. Fan, A.; Wang, J.; He, Y.; Perčić, M.; Vladimir, N.; Yang, L. Decarbonising Inland Ship Power System: Alternative Solution and Assessment Method. *Energy* **2021**, *226*, 120266. [CrossRef]
7. Zis, T.P.V.; Cullinane, K.; Ricci, S. Economic and Environmental Impacts of Scrubbers Investments in Shipping: A Multi-Sectoral Analysis. *Marit. Policy Manag.* **2022**, *49*, 1097–1115. [CrossRef]
8. Rong, H.; Teixeira, A.P.; Guedes Soares, C. Spatial Correlation Analysis of near Ship Collision Hotspots with Local Maritime Traffic Characteristics. *Reliab. Eng. Syst. Saf.* **2021**, *209*, 107463. [CrossRef]
9. Fang, S.; Xu, Y.; Wang, H.; Shang, C.; Feng, X. Robust Operation of Shipboard Microgrids With Multiple-Battery Energy Storage System Under Navigation Uncertainties. *IEEE Trans. Veh. Technol.* **2020**, *69*, 10531–10544. [CrossRef]
10. Li, Y.; Cui, J.; Zhang, X.; Yang, X. A Ship Route Planning Method under the Sailing Time Constraint. *J. Mar. Sci. Eng.* **2023**, *11*, 1242. [CrossRef]
11. De, A.; Wang, J.; Tiwari, M.K. Fuel Bunker Management Strategies Within Sustainable Container Shipping Operation Considering Disruption and Recovery Policies. *IEEE Trans. Eng. Manag.* **2021**, *68*, 1089–1111. [CrossRef]
12. Vettor, R.; Guedes Soares, C. Development of a Ship Weather Routing System. *Ocean Eng.* **2016**, *123*, 1–14. [CrossRef]
13. Chang, Y.-T.; Park, H.; Lee, S.; Kim, E. Have Emission Control Areas (ECAs) Harmed Port Efficiency in Europe? *Transp. Res. D Transp. Environ.* **2018**, *58*, 39–53. [CrossRef]
14. Ma, W.; Li, P.; Zhao, J. Joint Optimization of Ramp Closure, Lane Reorganization, and Signal Control Strategies for Freeway Mainline Closure Owing to Construction Zones. *Transp. B Transp. Dyn.* **2023**, *11*, 2231158. [CrossRef]
15. Skoglund, L.; Kuttenkeuler, J.; Rosén, A.; Ovegård, E. A Comparative Study of Deterministic and Ensemble Weather Forecasts for Weather Routing. *J. Mar. Sci. Technol.* **2015**, *20*, 429–441. [CrossRef]
16. Wu, Z.; Wang, S.; Yuan, Q.; Lou, N.; Qiu, S.; Bo, L.; Chen, X. Application of a Deep Learning-Based Discrete Weather Data Continuousization Model in Ship Route Optimization. *Ocean. Eng.* **2023**, *285*, 115435. [CrossRef]
17. Guo, W.; Zhang, X.; Wang, J.; Feng, H.; Tengecha, N.A. Traffic Organization Service for Maritime Autonomous Surface Ships (MASS) with Different Degrees of Autonomy. *J. Mar. Sci. Eng.* **2022**, *10*, 1889. [CrossRef]
18. Zhang, C.; Liu, S.; Guo, M.; Liu, Y. A Novel Ship Trajectory Clustering Analysis and Anomaly Detection Method Based on AIS Data. *Ocean Eng.* **2023**, *288*, 116082. [CrossRef]
19. Brynolf, S.; Magnusson, M.; Fridell, E.; Andersson, K. Compliance Possibilities for the Future ECA Regulations through the Use of Abatement Technologies or Change of Fuels. *Transp. Res. D Transp. Environ.* **2014**, *28*, 6–18. [CrossRef]
20. Jin, F.; Cheng, B.; Luo, W. Data-Driven Based Path Planning of Underwater Vehicles Under Local Flow Field. *J. Mar. Sci. Eng.* **2024**, *12*, 2147. [CrossRef]
21. Zhao, J.; Chen, Y.; Zhou, Z.; Zhao, J.; Wang, S.; Chen, X. Multiship Speed Measurement Method Based on Machine Vision and Drone Images. *IEEE Trans. Instrum. Meas.* **2023**, *72*, 2513112. [CrossRef]
22. Gao, D.; Zhu, Y.; Zhang, J.; He, Y.; Yan, K.; Yan, B. A Novel MP-LSTM Method for Ship Trajectory Prediction Based on AIS Data. *Ocean Eng.* **2021**, *228*, 108956. [CrossRef]
23. Murray, B.; Perera, L.P. An AIS-Based Deep Learning Framework for Regional Ship Behavior Prediction. *Reliab. Eng. Syst. Saf.* **2021**, *215*, 107819. [CrossRef]
24. Gu, Q.; Zhen, R.; Liu, J.; Li, C. An Improved RRT Algorithm Based on Prior AIS Information and DP Compression for Ship Path Planning. *Ocean Eng.* **2023**, *279*, 114595. [CrossRef]

25. Park, J.; Choi, M. A K-Means Clustering Algorithm to Determine Representative Operational Profiles of a Ship Using AIS Data. *J. Mar. Sci. Eng.* **2022**, *10*, 1245. [CrossRef]
26. Chen, S.; Huang, Y.; Lu, W. Anomaly Detection and Restoration for AIS Raw Data. *Wirel. Commun. Mob. Comput.* **2022**, *2022*, 5954483. [CrossRef]
27. Sang, H.; You, Y.; Sun, X.; Zhou, Y.; Liu, F. The Hybrid Path Planning Algorithm Based on Improved A* and Artificial Potential Field for Unmanned Surface Vehicle Formations. *Ocean Eng.* **2021**, *223*, 108709. [CrossRef]
28. Vettor, R.; Guedes Soares, C. Rough Weather Avoidance Effect on the Wave Climate Experienced by Oceangoing Vessels. *Appl. Ocean Res.* **2016**, *59*, 606–615. [CrossRef]
29. Koenig, S.; Likhachev, M.; Furcy, D. Lifelong Planning A∗. *Artif. Intell.* **2004**, *155*, 93–146. [CrossRef]
30. Koenig, S.; Likhachev, M. Fast Replanning for Navigation in Unknown Terrain. *IEEE Trans. Robot.* **2005**, *21*, 354–363. [CrossRef]
31. Saranya, C.; Unnikrishnan, M.; Ali, S.A.; Sheela, D.S.; Lalithambika, D.V.R. Terrain Based D∗ Algorithm for Path Planning. *IFAC-Pap.* **2016**, *49*, 178–182. [CrossRef]
32. Xing, B.; Yu, M.; Liu, Z.; Tan, Y.; Sun, Y.; Li, B. A Review of Path Planning for Unmanned Surface Vehicles. *J. Mar. Sci. Eng.* **2023**, *11*, 1556. [CrossRef]
33. Luo, J.; Zhuang, J.; Jin, M.; Xu, F.; Su, Y. An Energy-Efficient Path Planning Method for Unmanned Surface Vehicle in a Time-Variant Maritime Environment. *Ocean Eng.* **2024**, *301*, 117544. [CrossRef]
34. Wang, H.; Lang, X.; Mao, W. Voyage Optimization Combining Genetic Algorithm and Dynamic Programming for Fuel/Emissions Reduction. *Transp. Res. D Transp. Environ.* **2021**, *90*, 102670. [CrossRef]
35. Prpić-Oršić, J.; Vettor, R.; Faltinsen, O.M.; Guedes Soares, C. The Influence of Route Choice and Operating Conditions on Fuel Consumption and CO2 Emission of Ships. *J. Mar. Sci. Technol.* **2016**, *21*, 434–457. [CrossRef]
36. Liu, H.; Shan, Q.; Cao, Y.; Xu, Q. Global Path Planning of Unmanned Surface Vehicle in Complex Sea Areas Based on Improved Streamline Method. *J. Mar. Sci. Eng.* **2024**, *12*, 1324. [CrossRef]
37. Zhang, Y.; Shi, G.; Liu, J. Dynamic Energy-Efficient Path Planning of Unmanned Surface Vehicle under Time-Varying Current and Wind. *J. Mar. Sci. Eng.* **2022**, *10*, 759. [CrossRef]
38. Spyrou-Sioula, K.; Kontopoulos, I.; Kaklis, D.; Makris, A.; Tserpes, K.; Eirinakis, P.; Oikonomou, F. AIS-Enabled Weather Routing for Cargo Loss Prevention. *J. Mar. Sci. Eng.* **2022**, *10*, 1755. [CrossRef]
39. Rong, H.; Teixeira, A.P.; Guedes Soares, C. Data Mining Approach to Shipping Route Characterization and Anomaly Detection Based on AIS Data. *Ocean Eng.* **2020**, *198*, 106936. [CrossRef]
40. Song, Z.; Zhang, J.; Tian, W.; Guedes Soares, C. A Multi-Objective Ship Voyage Optimisation Method within Sulfur Emission Control Zones. *Ocean Eng.* **2025**, *319*, 120192. [CrossRef]
41. Sha, H.; Zhen, H.; Zhu, L. The Whole Process Route Planning Algorithm Based on AIS Spatio-Temporal Big Data Analysis. *Ships Offshore Struct.* **2024**, *20*, 912–926. [CrossRef]
42. Ankerst, M.; Breunig, M.M.; Kriegel, H.-P.; Sander, J. OPTICS: Ordering Points to Identify the Clustering Structure. *Sigmod Rec.* **1999**, *28*, 49–60. [CrossRef]
43. Douglas, D.H.; Peucker, T.K. Algorithms for the Reduction of the Number of Points Required to Represent a Digitized Line or Its Caricature. *Cartographica* **1973**, *10*, 112–122. [CrossRef]
44. Hart, P.; Nilsson, N.; Raphael, B. A Formal Basis for the Heuristic Determination of Minimum Cost Paths. *IEEE Trans. Syst. Sci. Cybern.* **1968**, *4*, 100–107. [CrossRef]
45. Song, Z.; Zhang, J.; Wu, D.; Tian, W. A Novel Path Planning Algorithm for Ships in Dynamic Current Environments. *Ocean Eng.* **2023**, *288*, 116091. [CrossRef]
46. Wang, H.; Mao, W.; Eriksson, L. A Three-Dimensional Dijkstra's Algorithm for Multi-Objective Ship Voyage Optimization. *Ocean Eng.* **2019**, *186*, 106131. [CrossRef]
47. Lang, X.; Mao, W. A Semi-Empirical Model for Ship Speed Loss Prediction at Head Sea and Its Validation by Full-Scale Measurements. *Ocean Eng.* **2020**, *209*, 107494. [CrossRef]
48. Acciaro, M. Real Option Analysis for Environmental Compliance: LNG and Emission Control Areas. *Transp. Res. D Transp. Environ.* **2014**, *28*, 41–50. [CrossRef]
49. Ma, W.; Lu, T.; Ma, D.; Wang, D.; Qu, F. Ship Route and Speed Multi-Objective Optimization Considering Weather Conditions and Emission Control Area Regulations. *Marit. Policy Manag.* **2021**, *48*, 1053–1068. [CrossRef]
50. Koenig, S.; Likhachev, M. Real-Time Adaptive A*. In Proceedings of the Fifth International Joint Conference on Autonomous Agents and Multiagent Systems, Hakodate, Japan, 8 May 2006; ACM: New York, NY, USA, 2006; pp. 281–288.

Disclaimer/Publisher's Note: The statements, opinions and data contained in all publications are solely those of the individual author(s) and contributor(s) and not of MDPI and/or the editor(s). MDPI and/or the editor(s) disclaim responsibility for any injury to people or property resulting from any ideas, methods, instructions or products referred to in the content.